IOP Publishing Journal of Physics: Condensed Matter
J. Phys.: Condens. Matter **32** (2020) 235701 (7pp) https://doi.org/10.1088/1361-648X/ab7871

Topological supersolidity of dipolar Fermi gases in a spin-dependent optical lattice

Huan-Yu Wang[1,2], Zhen Zheng[3], Lin Zhuang[4,8], Yong-Hang Tai[5,6], Jun-Sheng Shi[5] and Wu-Ming Liu[1,2,7]

[1] Beijing National Laboratory for Condensed Matter Physics, Institute of Physics, Chinese Academy of Sciences, Beijing 100190, People's Republic of China
[2] School of Physical Sciences, University of Chinese Academy of Sciences, Beijing 100190, People's Republic of China
[3] Department of Physics and HKU-UCAS Joint Institute for Theoretical and Computational Physics at Hong Kong, The University of Hong Kong, Pokfulam Road, Hong Kong, People's Republic of China
[4] School of Physics, Sun Yat-Sen University, Guangzhou 510275, People's Republic of China
[5] Yunnan Key Laboratory of Opto-electronic Information Technology, Yunnan Normal University, Kunming, People's Republic of China
[6] Institute for Intelligent Systems Research and Innovation, Deakin University, Geelong, VIC, Australia
[7] Songshan Lake Materials Laboratory, Dongguan, Guanddong 523808, People's Republic of China

E-mail: stszhl@mail.sysu.edu.cn

Received 4 November 2019, revised 10 February 2020
Accepted for publication 20 February 2020
Published 12 March 2020

Abstract

We investigate the topological supersolid states of dipolar Fermi gases trapped in a spin-dependent 2D optical lattice. Our results show that topological supersolid states can be achieved via the combination of topological superfluid states with the stripe order. Different from the general held belief that supersolid state in fermionic system can only survive with simultaneous coexistence of the repulsive and attractive dipolar interaction. We demonstrate that it can be maintained when the dipolar interaction is attractive in both x and y direction. By adjusting the ratio of hopping amplitude between different directions and dipolar interaction strength U, the system will undergo a phase transition among $p_x + ip_y$ superfluid state, p_y-wave superfluid state, and the topological supersolid state. The supersolid state in the attractive environment is proved to be stable by the positive sign of the inverse compressibility. We also design an experimental protocol to realize the staggered next-next-nearest-neighbor hopping via the laser assisted tunneling technique, which is the key to simulate the spin-dependent potential.

Keywords: topological supersolid state, anistropic dipolar interaction, stripe order

(Some figures may appear in colour only in the online journal)

1. Introduction

Supersolid (SS) states can be defined as a combination of superfluid states with off-diagonal long range order and solid states with diagonal orders, the concept of which was first emerged in the context of solid ^{4}He [1–7]. As a novel state of matter, the supersolid state exhibits unconventional properties and its realization method has long been an intriguing task for theoretical and experimental physicists [8–50]. Recent works by Li *et al* [51] and Léonard *et al* [52] realize periodical density modulation (stripes) in Bose–Einstein condensates (BEC), which shed light on how to produce supersolid states in a bosonic system. For fermionic systems, the most promising candidates are dipolar Fermi gases due to the anisotropic features [53, 54]. By tilting the orientation of dipoles, dipolar interaction can be decoupled to a repulsive part and an attractive part in separated directions, which is the key to form the stripe order [55] and the superfluid order. The two orders compete with each other, and the supersolid state is predicted to arise at moderate interaction strength. However, the

[8] Author to whom any correspondence must be addressed.

corresponding supersolid state is trivial in topology, and the parameter space to maintain supersolid is also quite limited.

In this work, we investigate the topological supersolid state of dipolar Fermi gases in a 2D optical lattice with staggered next-next-nearest-neighbor hopping, which is equivalent to a spin-dependent potential. We exhibit that our hopping formalism can cooperate with dipolar coupling between different optical lattice sites to generate a new type of stripe order which no longer relies on the repulsive part of dipolar interaction. When the dipolar interaction is decoupled to attractive parts in both x and y directions and the two parts are balanced in strength, the $p_x + ip_y$ topological superfluid state arises, which can be combined with the stripe order, yielding the topological supersolid states. The topological features are characterized by Chern numbers as well as the existence of the edge states. Furthermore, we prove that the topological supersolid state is stable via the positive sign of the inverse compressibility. The simplicity of our lattice model makes it reliable and feasible in realization via the laser assisted tunneling technique.

2. Model and results

We consider ^{161}Dy atoms confined in a 2D optical lattice, with the lattice potential given by $V_{\rm opt}(\mathbf{r}) = V_{\rm 2D}[\sin^2(\pi x/a) + \sin^2(\pi y/a)]$. $V_{\rm 2D}$ is the trap strength, and $a = 450$ nm is the lattice constant [56]. The next-next-nearest-neighbor hopping can be induced by the laser assisted tunneling technique [57, 58] with the phase π and 0 staggeredly loaded along the x direction, which naturally leads to two effective types of atoms (A, B). Along the y direction, hopping is uniform, and A, B types of atoms share the same lattice structure (see figure 1(b)). Thus, the lattice potential is equivalent to a spin-dependent one with A (B) sites regarded as pseudospin index respectively. We assume ^{161}Dy atoms are prepared in its lowest hyperfine nuclear spin states and spin degrees of freedom are frozen out. The system can be described by a spinless Fermi–Hubbard model,

$$\mathcal{H}' = \sum_i \left(-t_x c_i^\dagger c_{i+2\hat{e}_x} e^{i\pi i_x} - t_y c_i^\dagger c_{i+\hat{e}_y} - \mu c_i^\dagger c_i + h.c.\right) + \frac{1}{2}\sum_{i\neq j} V_{ij} c_i^\dagger c_j^\dagger c_j c_i \tag{1}$$

where $c_i^\dagger$ (c_i) creates (annihilates) a fermion at site R_i. t_x, t_y is the amplitude of hopping in x and y direction, and is denoted by $t_x \equiv gt$, $t_y \equiv t$, and the explicit form of g can be seen in section experiment realization and effective Hamiltonian derivation. t is also utilized as the unitary of energy in this work. Dipoles are aligned in parallel by external electric field $\boldsymbol{E}$ into a direction which is inside the plane, and keeps an angle ϕ with respect to x axis. The interaction between dipoles moments $\mathbf{d}$ separated by $\mathbf{r}$ is given by

$$U_{\rm dd} = -\frac{1}{|\mathbf{r}|^3}\left(3\left(\mathbf{d}\cdot\hat{\mathbf{r}}\right)\left(\mathbf{d}\cdot\hat{\mathbf{r}}\right) - \mathbf{d}\cdot\mathbf{d}\right) = \frac{\mathbf{d}^2}{|\mathbf{r}|^3}(1 - 3\cos(\phi-\theta)^2) \tag{2}$$

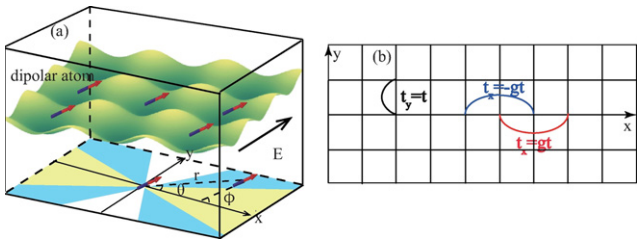

Figure 1. (a) Dipolar Fermi gases in a 2D optical lattice with staggered next-next-nearest-neighbor hopping and its interaction projection. The dipoles form an angle ϕ with respect to x axis, and θ is the angle between the separation of dipole moments, $\mathbf{r}$, and x axis. $\boldsymbol{E}$ is the external field. In the yellow area, the dipolar interaction decouples to an attractive part in x direction and a repulsive part in y direction. In the blue area, the dipolar interaction decouples to attractive parts in both x and y directions. In the white area, the dipolar interaction decouples to an attractive part in y direction and a repulsive part in x direction. (b) The schematic diagram of the staggered next-next-nearest-neighbor hopping in the x–y plane.

A schematic picture of the system is shown in figure 1(a). Experimentally, our Hamiltonian provides three tunable parameters: (i) the hopping ratio g can be controlled by adjusting the Rabi frequency in the laser-assisted tunneling technique. (ii) The dimensionless coupling strength is given by:

$$U \equiv |d|^2/(ta^3) \tag{3}$$

$|d|$ is the amplitude of dipole moment. The amplitude of U characterize the strength of dipolar coupling. $V_{i,j}$ in equation (1) is decided by $U_{\rm dd}$, which can be changed by manipulating the strength of lattice trap. (iii) The orientation of dipole moments ϕ, which can be tilted by external electric $\boldsymbol{E}$. The controllable parameter set $\{g, U, \phi\}$ can give rise to a phase diagram with rich physics.

Our results are obtained by the Bogoliubov-de Gennes (BdG) approach, with the order parameter determined by solving local minimum of free energy self-consistently. Within Hartree–Fock–Bogoliubov formalism, the interaction term can be decoupled to

$$V_{HF} = \Delta_{ij} c_i^\dagger c_j^\dagger + \Delta_{ij}^* c_j c_i + V_{ij}(\langle n_i\rangle c_j^\dagger c_j + \langle n_j\rangle c_i^\dagger c_i) + E_0 \tag{4}$$

where $E_0 = \frac{1}{2}\left(\sum_{i\neq j} - \frac{\Delta_{ij}^2}{V_{ij}} - V_{ij}\langle n_i\rangle\langle n_j\rangle\right)$. Since the dipole–dipole coupling is strongest between nearest neighbors, and decays as a function of distance between lattice sites to the order $\frac{1}{|r|^3}$, we consider the pairing to be between nearest neighbors [26, 59–61]. We describe the superfluid order parameter as $\Delta_{ij} = V_{ij}\langle c_i c_j\rangle\delta_{j,i+\hat{e}_\lambda}$ with $\lambda = x, y$. To manifest the stripe order, we assume $\langle n_i\rangle = \frac{1}{2} + e^{i\boldsymbol{Q}\cdot\mathbf{R}_i}C$, $|C| \leqslant \frac{1}{2}$. $\boldsymbol{Q}$ indicates the periodicity of density pattern. For the in plane electric dipoles, $\boldsymbol{Q}$ is assumed to be $[\pi, 0]$ [62, 63]. The free energy can be given by: $\Omega = TS$, and the action S is of the form $S = \int d\tau \sum_i c_i^\dagger(\tau)\frac{\partial}{\partial\tau}c_i(\tau) + H(\tau)$. By Fourier transformation and summing over the Matsubara frequency, we obtain the thermodynamic potential:

$$\Omega = \tilde{E}_0 - T\sum_{n,\mathbf{k}} \ln[1 + \exp(-E_n(\mathbf{k})/T)] + \sum_{\mathbf{k}} \widetilde{\kappa} \tag{5}$$

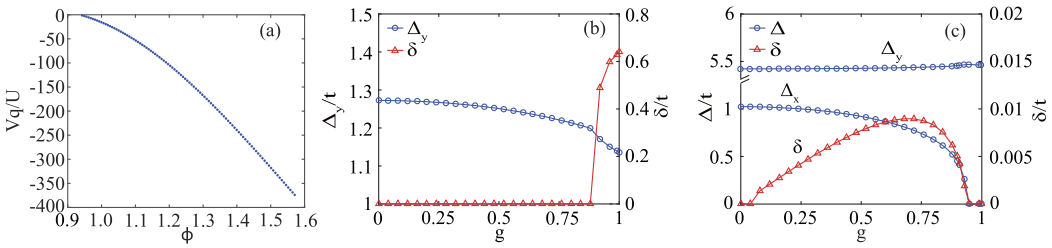

Figure 2. (a) V_q/U varies as a function of dipole orientation $\phi \in [0.3\pi, 0.5\pi]$. (b, c) The pairing gap Δ_x, Δ_y, and stripe gap δ change as a function of hopping ratio g for different orientations of dipoles ϕ and interaction strength U. (b) Pairing gap Δ_y and stripe gap δ at $\phi = 0.3\pi$, $U = 5$. (c) Pairing gap $\Delta_x + \mathrm{i}\Delta_y$ and stripe gap δ at $\phi = 0.26\pi$, $U = 30$.

where $\widetilde{\kappa} = -t_y \cos(k_y a)$ and $E_n(\mathbf{k})$ is the eigenvalue of $H_{\mathrm{BdG}}(\mathbf{k})$. $\tilde{E}_0 = \frac{-1}{2}\left(\sum_\lambda \frac{\Delta_\lambda^2}{V_\lambda} + \frac{\delta^2}{V_Q}\right)$, $\lambda = x, y$, and V_λ takes the form:

$$V_{x(y)} = V_{ij}\delta_{j=i+\hat{e}_{x(y)}} \tag{6}$$

As we consider zero temperature limit, above thermodynamical potential reduces to:

$$\Omega_{(T=0)} = \tilde{E}_0 + \sum_{n,\mathbf{k}} E_n(\mathbf{k})\theta(-E_n(\mathbf{k})) + \sum_{\mathbf{k}} \widetilde{\kappa} \tag{7}$$

where $\theta(-E_n(\mathbf{k}))$ is the Heaviside step function. On the basis of $\Psi = (c_{\mathbf{k}}, c_{\mathbf{k}+\boldsymbol{Q}}, c^\dagger_{-\mathbf{k}}, c^\dagger_{-\mathbf{k}-\boldsymbol{Q}})$, we have $H_{\mathrm{BdG}}(\mathbf{k})$ can be described as:

$$H_{\mathrm{BdG}}(\boldsymbol{k}) = \begin{pmatrix} A_{\boldsymbol{k}} & D_{\boldsymbol{k}} \\ D^\dagger_{\boldsymbol{k}} & -A_{\boldsymbol{k}} \end{pmatrix} \tag{8}$$

in which

$$A_{\boldsymbol{k}} = -\frac{1}{2}t_y \cos(k_y a)\boldsymbol{I} + \frac{1}{4}\left[\delta - 2t_x \cos(2k_x a)\right]\sigma_x \tag{9}$$

$$D_{\boldsymbol{k}} = \frac{i}{2}(\Delta_x \sin(k_x a)\sigma_z + \mathrm{i}\Delta_y \sin(k_y a)\boldsymbol{I}) \tag{10}$$

where $\boldsymbol{I}$ is the identity matrix. $\delta = V_{\boldsymbol{Q}} C$ with $V_Q = \int \mathrm{d}\boldsymbol{r} V_{ij}(\boldsymbol{r})\mathrm{e}^{\mathrm{i}\boldsymbol{Q}\boldsymbol{r}}$, which characterizes the amplitude of the stripe order parameter. The self consistent gap equation can be deduced via $\frac{\partial\Omega}{\partial\Delta} = 0$, $\frac{\partial\Omega}{\partial\delta} = 0$. Need to mention that since one dipole interacts with many others, given the lattice scale large enough, the effective dimension of the system can be so high that the fluctuation impacts are suppressed. Hence, we consider 500×500 lattice sites in calculating the Hartree term to ensure the validity of the mean field method.

The orientation of dipoles ϕ, hopping ratio g and interaction strength U determine much of the physics of the system. When $\phi > 0.3\pi$, the dipolar interaction can be projected to an attractive part in y direction, which results in a superfluid order Δ_y, and a repulsive part in x direction, which yields a stripe order δ. The two order parameters compete with each other and the system will undergo phase transitions with the change of interacting strength U. For example, at $\phi = 0.35\pi$, superfluid order Δ_y is observed with small interaction strength U. As U is enhanced, stripe order δ gradually appears, and will dominate at large interaction strength, which contributes to a Mott insulator. With the moderate value of interaction strength, the coexistence of the stripe order δ and the superfluid order Δ_y defines a supersolid state. Besides, we also present that in figure 2(a) as $\phi \to \pi/2$, $|V_q|$ becomes quite large. As a consequence of which, stripe order get reinforced and can be obtained within small interaction strength U. Above supersolid states with repulsive dipolar coupling is similar to the previous work [26].

Since we are only interested in supersolid states in the attractive interaction region, we restrict the dipoles to be arranged in the region $0.3\pi > \phi > 0.2\pi$ (blue area in figure 1(a)). When ϕ is about 0.3π, the attractive interaction strength in x direction is much weaker than that in y direction, $V_x/V_y = 0.0379$, as a consequence of which pairing order y direction is manifested. By numerically locating the minimum of the free energy, we obtain the magnitude of pseudogap as a function of hopping ratio g at $U = 5$ (see figure 2(b)). It can be seen that the pairing gap Δ_y is insensitive to the hopping ratio g and the stripe gap δ emerges for $g > 0.92$, indicating a supersolid state. To investigate the origination of the stripe order with respect to g, we consider the expression of $A_{\mathbf{k}}$ in equation (9), where term $\frac{1}{4}\left[\delta - 2t_x \cos(2k_x a)\right]\sigma_x$ is equivalent to an effective $\mathbf{k}$-dependent Zeeman field h. The dipolar interaction provides the coupling between different sites of the sublattice (or pseudospins) A, B, which is equivalent to a coupling between spins. As a response to the magnetic field h, pseudospin wave will be formed and it corresponds to the stripe order. It is need to mention that when the dipolar interaction is absent, the system is in fact constructed by the two isolated sublattices A and B without inter-sublattice coupling. For the sake of spin balance, the two sublattices A and B, although the existence of a staggered relative π phase, up and down pseudospin will form a spatial uniform pattern. Thus the stripe order is formed spontaneously.

As the orientation of dipoles ϕ reduces to 0.26π, we have $|V_x/V_y| = 0.6829, |V_Q/V_y| = 0.1989$. The superfluid order Δ_x appears, and is accompanied with $\frac{\pi}{2}$ phase relative to that in y direction. The superfluid order Δ_x, Δ_y and stripe order δ compete with each other as a function of hopping ratio g and interaction strength U (see figure 2(c)). Numerical results show that the stripe order δ can still be detected at large interaction strength and the simultaneous coexistence of the topological superfluid order $\Delta_x + \mathrm{i}\Delta_y$ and the stripe order δ characterises a topological supersolid (TSS) state. Furthermore, it can be seen that with the increasing of the hopping ratio g, superfluid order parameter Δ_x gradually shrinks due to the reduction of U/g along the x direction and vanishes at $g = 0.96$. Likewise, the stripe order parameter reaches a peak at $g = 0.7$, and

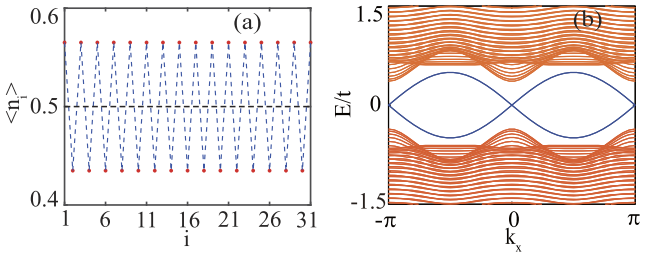

Figure 3. (a) Average density modulation of the topological supersolid states in x direction with $g = 0.3$, $\phi = 0.26\pi$, $U = 30$. (b) Edge states of topological supersolid states with $g = 0.3$, $\phi = 0.26\pi$, $U = 30$. Open boundary conditions are used in y direction.

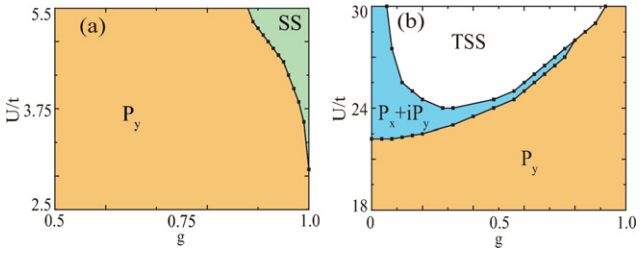

Figure 4. The phase diagram as a function of hopping ratio g and interaction strength U. (a) The supersolid state (SS) and the p-wave superfluid state (p_y) survive in the attractive interaction region for $\phi = 0.3\pi$. (b) The $p_x + ip_y$-wave topological superfluid state and the topological supersolid state (TSS) emerge at large interaction strength for $\phi = 0.26\pi$.

will decay for $g > 0.7$. To manifest the stripe order in topological supersolid states, we calculate average density at ith site in the x direction with $g = 0.3$, $\phi = 0.26\pi$, $U = 30$ (see figure 3(a)). A periodical density modulation $\langle n_{i+1}\rangle - \langle n_i\rangle = C(e^{i\boldsymbol{Q}\cdot\mathbf{R_{i+1}}} - e^{i\boldsymbol{Q}\cdot\mathbf{R_i}}) = 0.1302$ is observed in x direction.

We map out the phase diagram as a function of interaction strength U and hopping ratio g at zero temperature as shown in figure 4. For $\phi = 0.3\pi$ (see figure 4(a)), at modest interaction strength ($U < 3.1$), stripe order is absent for all cases of g, and the system is a p_y wave superfluid state. With the increasing of U, stripe order gradually emerges, and the system becomes a supersolid state. Phase diagram for $\phi = 0.26\pi$ is shown in figure 4(b). Topological superfluid states and topological supersolid states exist at large coupling strength, and can transfer to each other with the tuning of hopping ratio g. To investigate the topological classification of topological supersolid states, we denote the particle-hole reversal (Ξ) operator as: $\Xi = \sigma_x \boldsymbol{K}$, where $\boldsymbol{K}$ is the complex conjugate operator. Thus, we have $\Xi H_{\mathrm{BdG}}(\mathbf{k})\Xi^{-1} = -H_{\mathrm{BdG}}(-\mathbf{k})$. Since $\Xi^2 = 1$ and the time-reversal symmetry is broken due to the $\pi/2$ relative phase in the superfluid order parameter, we clarify the topological supersolid state as D class, which can be characterized by the Z index [64–67], Chern number. In details, the Chern number can be given by:

$$C = \frac{1}{2\pi}\int_{BZ} \mathrm{d}k_x \mathrm{d}k_y [\partial k_x A_y - \partial k_y A_x] \tag{11}$$

where the Berry connection $A_i(k) = i\sum_{n\in\text{filled}}\langle u_{n,k}|\partial k_i|u_{n,k}\rangle$, $|u_{n,k}\rangle$ is the eigenstate of nth filled bands of $H_{\mathrm{BdG}}(k)$. Numerically, we utilize the efficient method as shown in reference [68]. It is exhibited that the Chern number changes with varying hopping ratio g with $\phi = 0.26\pi$, $U = 30$. Numerical results exhibit that $C = 1$ for $g < 0.96$, which is in consistence with our results in figure 2(c), where $g < 0.06$ depicts a topological superfluid state, and $0.06 < g < 0.96$ depicts a topological supersolid states. For $0.96 < g < 1$, $C = 0$, which means the p_y-wave superfluid state topological trivial. Indeed, since the topological supersolid states are formed with attractive dipolar interaction, where $p_x + ip_y$ wave topological superfluid order take the dominant place, we can adiabatically tilt stripe order to 0 without closing the gaps, which means topological supersolid states are topological equivalent with $p_x + ip_y$ topological superfluid phase. In figure 3(b),

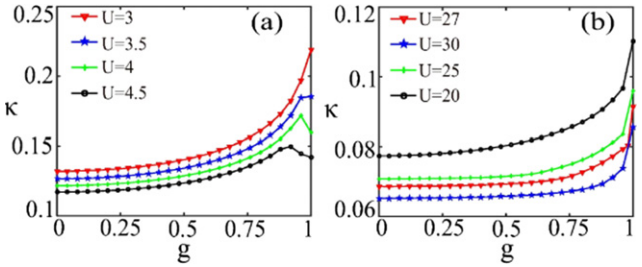

Figure 5. The compressibility κ varies as a function of the hopping ratio g with different interaction strength U and dipole orientation ϕ. (a) $\phi = 0.3\pi$. (b) $\phi = 0.26\pi$.

we present the edge state for topological supersolid states with $\phi = 0.26\pi$, $U = 30$, $g = 0.3$. Thus, we have our topological nontrivial supersolid states proved in both geometric and quantitative aspect.

The stability of the supersolid state in the attractive interaction region can be justified by the sign of inverse compressibility [69–71]

$$\kappa^{-1} = n^2\frac{\partial\mu}{\partial n} = -n^2\frac{\partial^2\Omega_{(T=0)}}{\partial n^2}|_{n=n_0}, \quad n_0 = \frac{1}{2}. \tag{12}$$

where $\Omega_{(T=0)}$ is the thermodynamic potential as shown in equation (7), and thus κ can be obtained numerically. The positive sign of inverse compressibility suggests that the system will not collapse [69], which is frequently used in Hubbard model to describe the stability and emergence of Mott insulator phase [70]. As adaptations, we extend it to our long range Hubbard model with dipolar coupling. Numerical results for the compressibility as a function of hopping ratio g with various interaction strength U for $\phi = 0.3\pi$, $\phi = 0.26\pi$ are shown in figure 5(a) and (b). It can be seen that the compressibility is always positive, which implies that the supersolid state and the topological supersolid state will not collapse. Besides, from figure 5(a), it can be seen that the compressibility increases with the augment of g at first, and will encounter a reduction as $g \to 1$, which indicates the stripe order begins to show up. For $\phi = 0.3\pi$, the stripe order dominates at large interaction strength $U = 15$, indicating a Mott insulator state with density pattern, which is non compressible with $\kappa = 0$.

2.1. Experiment realization and effective Hamiltonian derivation

In order to generate strong enough dipolar interaction strength, we consider the hyperfine state $|F, mF\rangle = |21/2, -21/2\rangle$ of ^{161}Dy dipolar atoms. The atoms are confined in a 2D optical lattice with lattice constant $a = 450$ nm [56], where the bare tunneling is inhibited by the energy offset Δ [72] and the staggered next-next-nearest tunneling is introduced via the laser-assisted tunneling technique [57, 58] (see figure 6(a)). In details, two far-detuned Raman beams (k_1, ω_1), (k_2, ω_2) are utilized with the difference of laser frequency prefixed to be $\delta\omega = \omega_1 - \omega_2 = 2\Delta$, a time dependent oscillating potential can be formed $V(r, t) = V_0(\cos(\delta k \cdot r) - \omega t)$, $\delta k = k_1 - k_2$, V_0 is the trap strength. The dipoles trapped in 2D optical lattice with Raman coupling can be described as:

$$H = \int \mathrm{d}^2 r \hat{\psi}^\dagger(r) \left[-\frac{\hbar^2 \Delta^2}{2m} + V_{\mathrm{opt}}(x, y) + 2\Delta x + V_0 \cos(\delta k \cdot r - \omega t) \right] \hat{\psi}(r) + \frac{1}{2} \iint \mathrm{d}^2 r_1 \mathrm{d}^2 r_2 \hat{\psi}^\dagger(r_1) \hat{\psi}^\dagger(r_2) U_{\mathrm{dd}}(r_1 - r_2) \hat{\psi}(r_1) \hat{\psi}(r_2) \tag{13}$$

where U_{dd} depicts the dipolar coupling in real space, and ω is the oscillating frequency. When $U_{\mathrm{dd}} \ll \Delta$, we can take the following basis: $m, n\rangle = |m\rangle \otimes |n\rangle \equiv w(r - R_{m,n})$, where $|m\rangle$ is the Wannier–Stark state centered at m, and $|n\rangle$ is the Wannier state centered at n. Thus, in a second quantization representation, the interaction term can be regarded as $H_{\mathrm{int}} = \sum_{i,j} V_{ij} c_i^\dagger c_j^\dagger c_j c_i$ and

$$V_{i,j} = \int \mathrm{d}^2 r_1 \mathrm{d}^2 r_2 w^*(r - R_i) w^*(r - R_j) U_{\mathrm{dd}}(r_1 - r_2) \times w(r_1 - R_j) w(r_2 - R_i) \tag{14}$$

Above results account for the interaction part in the effective model equation (1). For the tunneling part, the Raman laser induced tunneling takes the form:

$$J = \langle m, n | V_0 \cos(\delta k \cdot r - \omega t) | m + 2, n \rangle = \langle 0, 0 | V_0 \cos(\delta k \cdot (r + R_{m,n}) - \omega t) | 2, 0 \rangle \tag{15}$$

Assume $\delta k \cdot r = k_x x + k_y y$, $\theta_{m,n} = \omega t - \delta k \cdot R_{m,n}$. Then $J = V_0 \cos\theta_{m,n} \langle 0 | \cos(k_x x) | 2 \rangle$. Define $\langle 0 | \cos(k_x x) | 2 \rangle$ as J_2, and in second quantization presentation, the tunneling parts take the form:

$$\widetilde{H}_0 = \sum_{m,n} (2\Delta m + V_0 \cos \theta_{m,n}) |m, n\rangle\langle m, n| + (V_0 \cos \theta_{m,n} J_2 |m + 2, n\rangle\langle m, n| + h.c.) + (t_y |m, n + 1\rangle\langle m, n| + h.c.) \tag{16}$$

where $t_y = \int \mathrm{d}^2 r w^*(r - (R_{m,n} + \widehat{e}_y)) \left[\frac{-\hbar^2 \Delta^2}{2m} + V_{\mathrm{opt}}(x, y) \right] w(r - R_{m,n})$. By rotating transformation $U(t) = \sum_{m,n} \mathrm{e}^{-\mathrm{i}\gamma_{m,n}} |m, n\rangle\langle m, n|$, $\gamma_{m,n} = m\omega t + \frac{V_0}{\omega} \sin \theta_{m,n}$, we obtain the transformed tunneling term in x direction.

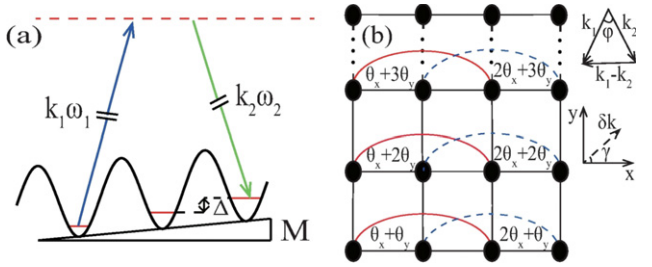

Figure 6. (a) Experimental setup for staggered next-next-nearest-neighbor tunneling via Raman laser assisted tunneling technique. (k_1, ω_1), (k_2, ω_2) are two far detuned Raman lasers, Δ is the energy offset induced by gradient magnetic field $\boldsymbol{M}$. (b) The phase accumulated in the Raman laser assisted tunneling process. φ is the angle between two laser beams, γ is the angle between $\delta\mathbf{k}$ and x axis.

$$\widetilde{H}'_{0x} = V_0 \cos \theta_{m,n} J_2 \mathrm{e}^{\mathrm{i}(\gamma_{m+2,n} - \gamma_{m,n})} |m + 2, n\rangle\langle m, n| + h.c. \tag{17}$$

By rotating wave approximation, we shall obtain the time independent effective tunneling in x direction:

$$\widetilde{H}^{eff}_{0x} = t'_x |m + 2, n\rangle\langle m, n| + h.c. \tag{18}$$

where $t'_x = \frac{J_2}{2} V_0 \mathrm{e}^{2\mathrm{i}\delta k \cdot R_{m,n}} (\mathcal{J}_3(\Gamma) - \mathcal{J}_1(\Gamma))$, $\mathcal{J}_i(\Gamma)$ is the ith Bessel function, and $\Gamma = \frac{2V_0}{\omega} \sin(-k_x a)$, a is the lattice constant. We deal with y direction tunneling in a similar way and the time independent effective hopping amplitude $t'_y = t_y \mathcal{J}_0(\Gamma')$, $\Gamma' = \frac{2V_0}{\omega} \sin\left(\frac{k_y a}{2}\right)$. Above results present how to induce the position dependent phase via laser assisted tunneling. For our staggered next-next-nearest hopping, we shall take

$$2\delta\mathrm{k} \cdot \mathrm{R} = m\theta_x + n\theta_y = \pi, \quad \theta_x = 2\pi |\sin(\varphi/2)| \cos(\gamma), \quad \theta_y = 2\pi |\sin(\varphi/2)| \sin(\gamma) \tag{19}$$

Here φ is the angle between two laser beams and γ is the angle between $\delta\mathbf{k}$ and x axis (see figure 6(b)). To achieve our staggered next-next-nearest-neighbor hopping, we fix $\varphi = 2 \arcsin \frac{1}{4}$, and $\gamma = \pi$. Above results accounts for the Hamiltonian equation (1) in effective model. Meanwhile, according to the amplitude of effective hopping shown above, we shall obtain the explicit form $g = \frac{t'_x}{t'_y}$, which can be tilted by manipulating the Rabi frequency and the supersolid state can be detected through time of flight measurements [73–76].

3. Conclusion

In conclusion, we have investigated topological supersolid states of dipolar Fermi gases in a 2D optical lattice with staggered next-next-nearest-neighbor hopping. Our results bring up a new type of stripe order, and greatly enhanced the parameter space for detecting supersolid state. Topological phase transitions among topological supersolid states, topological superfluid states, p wave superfluid states with different coupling strength as well as hopping ratio g are shown. We also utilize the inverse compressibility to prove

that the topological supersolid state will not collapse at large coupling strength in the attractive environment. Meanwhile, the novel state, topological supersolid state, may have significant potential for quantum computing. Experiment proposals to simulate the topological supersolid state are also presented.

Acknowledgments

We are grateful to Lan Yin, Xu-Bo Zou, and Ru-Quan Wang for helpful discussions. This work was supported by the National Key R and D Program of China under grants No. 2016YFA0301500, NSFC under grants Nos. 1835013, 11728407, the Strategic Priority Research Program of the Chinese Academy of Sciences under grants Nos. XDB01020300, XDB21030300.

ORCID iDs

Huan-Yu Wang https://orcid.org/0000-0001-6571-4205
Zhen Zheng https://orcid.org/0000-0003-1902-1162
Lin Zhuang https://orcid.org/0000-0001-9396-149X
Wu-Ming Liu https://orcid.org/0000-0002-1179-2061

References

[1] Andreev A F and Lifshitz I M 1969 *Sov. Phys. JETP* **29** 1107
[2] Chester G V 1970 *Phys. Rev. A* **2** 256
[3] Leggett A J 1970 *Phys. Rev. Lett.* **25** 1543
[4] Bijlsma M J and Stoof H T C 1997 *Phys. Rev. B* **56** 14631
[5] Prokof'ev N and Svistunov B 2005 *Phys. Rev. Lett.* **94** 155302
[6] Pollet L, Boninsegni M, Kuklov A B, Prokof'ev N V, Svistunov B V and Troyer M 2008 *Phys. Rev. Lett.* **101** 097202
[7] Choi H, Kwon S, Kim D Y and Kim E 2010 *Nat. Phys.* **6** 424
[8] Batrouni G G and Scalettar R T 2000 *Phys. Rev. Lett.* **84** 1599
[9] Sengupta P, Pryadko L P, Alet F, Troyer M and Schmid G 2005 *Phys. Rev. Lett.* **94** 207202
[10] Wessel S and Troyer M 2005 *Phys. Rev. Lett.* **95** 127205
[11] Zhao E and Paramekanti A 2006 *Phys. Rev. Lett.* **96** 105303
[12] Lahaye T, Koch T, Fröhlich B, Fattori M, Metz J, Griesmaier A, Giovanazzi S and pfau T 2007 *Nature* **448** 672
[13] Rittner A S C and Reppy J D 2007 *Phys. Rev. Lett.* **98** 175302
[14] Danshita I and Sa de Melo C A R 2009 *Phys. Rev. Lett.* **103** 225301
[15] Tieleman O, Lazarides A and Smith C M 2011 *Phys. Rev. A* **83** 013627
[16] Li X, Liu W V and Lin C 2011 *Phys. Rev. A* **83** 021602(R)
[17] Ye J, Zhang J M, Liu W M, Zhang K, Li Y and Zhang W 2011 *Phys. Rev. A* **83** 051604(R)
[18] He L and Hofstetter W 2011 *Phys. Rev. A* **83** 053629
[19] Bühler A and Büchler H P 2011 *Phys. Rev. A* **84** 023607
[20] Bhongale S G, Mathey L, Tsai S W, Clark C W and Zhao E 2012 *Phys. Rev. Lett.* **108** 145301
[21] Henkel N, Cinti F, Jain P, Pupillo G and Pohl T 2012 *Phys. Rev. Lett.* **108** 265301
[22] Yao N Y, Laumann C R, Gorshkov A V, Bennett S D, Demler E, Zoller P and Lukin M D 2012 *Phys. Rev. Lett.* **109** 266804
[23] Macrí T, Maucher F, Cinti F and Pohl T 2013 *Phys. Rev. A* **87** 061602(R)
[24] Olson A J, Whitenack D L and Chen Y P 2013 *Phys. Rev. A* **88** 043609
[25] Mishra T, Pai R V and Mukerjee S 2014 *Phys. Rev. A* **89** 013615
[26] Zeng T S and Yin L 2014 *Phys. Rev. B* **89** 174511
[27] Ng K K 2015 *Phys. Rev. B* **91** 054516
[28] Han W, Juzeliunas G, Zhang W and Liu W M 2015 *Phys. Rev. A* **91** 013607
[29] Olsen R J 2015 *Phys. Rev. A* **91** 033602
[30] Zhang W, Yang Y, Guo L, Ding C and Scott T C 2015 *Phys. Rev. A* **91** 033613
[31] Robb G R M, Tesio E, Oppo G L, Firth W J, Ackemann T and Bonifacio R 2015 *Phys. Rev. Lett.* **114** 173903
[32] Lu Z K, Li Y, Petrov D S and Shlyapnikov G V 2015 *Phys. Rev. Lett.* **115** 075303
[33] Wu Z, Block J K and Bruun G M 2015 *Phys. Rev. B* **91** 224504
[34] Landig R, Hruby L, Dogra N, Landini M, Mottl R, Donner T and Esslinger T 2016 *Nature* **532** 476
[35] Zhang X F, Hu S, Pelster A and Eggert S 2016 *Phys. Rev. Lett.* **117** 193201
[36] Niederle A E, Morigi G and Rieger H 2016 *Phys. Rev. A* **94** 033607
[37] Keles A and Zhao E H 2016 *Phys. Rev. A* **94** 033616
[38] Camacho-Guardian A and Paredes R 2016 *Phys. Rev. A* **94** 043638
[39] Ostermann S, Piazza F and Ritsch H 2016 *Phys. Rev. X* **6** 021026
[40] Geissler A, Vasic I and Hofstetter W 2017 *Phys. Rev. A* **95** 063608
[41] Wang J G and Yang S J 2017 *Phys. Lett. A* **381** 752
[42] Hugel D, Strand H U R, Werner P and Pollet L 2017 *Phys. Rev. B* **96** 054431
[43] Sentef M A, Tokuno A, Georges A and Kollath C 2017 *Phys. Rev. Lett.* **118** 087002
[44] Mivehvar F, Ostermann S, Piazza F and Ritsch H 2018 *Phys. Rev. Lett.* **120** 123601
[45] Liao R Y 2018 *Phys. Rev. Lett.* **120** 140403
[46] Kollath C, Sheikhan A, Wolff S and Brennecke F 2016 *Phys. Rev. Lett.* **116** 060401
[47] Camacho-Guardian A, Paredes R and Caballero-Benitez S F 2017 *Phys. Rev. A* **96** 051602(R)
[48] Colella E, Citro R, Barsanti M, Rossini D and Chiofalo M L 2018 *Phys. Rev. B* **97** 134502
[49] Mivehvar F, Ritsch H and Piazza F 2017 *Phys. Rev. Lett.* **118** 073602
[50] Schlawin F and Jaksch D 2019 *Phys. Rev. Lett.* **123** 133601
[51] Li J R, Lee J, Huang W, Burchesky S, Shteynas B, Top F C, Jamison A O and Ketterle W 2017 *Nature* **543** 91
[52] Léonard J, Morales A, Zupancic P, Esslinger T and Donner T 2017 *Nature* **543** 87
[53] Chui S T 1995 *Phys. Rev. B* **51** 250
[54] Li Y and Wu C 2012 *Phys. Rev. B* **85** 205126
[55] Sun K, Wu C and Sarma S D 2010 *Phys. Rev. B* **82** 075105
[56] Lu M, Burdick N Q and Lev B L 2012 *Phys. Rev. Lett.* **108** 215301
[57] Aidelsburger M, Atala M, Lohse M, Barreiro J T, Paredes B and Bloch I 2013 *Phys. Rev. Lett.* **111** 185301
[58] Miyake H, Siviloglou G A, Kennedy C J, Burton W C and Ketterle W 2013 *Phys. Rev. Lett.* **111** 185302
[59] Li S, Dong B, Li H R, Li F L and Liu B 2019 (arxiv: 1904.09118)
[60] Liu B, Li X P, Yin L and Liu W V 2015 *Phys. Rev. Lett.* **114** 045302
[61] Dominguez-Castro G A and Paredes R 2018 (arxiv: 1806.04268)
[62] Gadsbølle A L and Bruun G M 2012 *Phys. Rev. A* **85** 021604(R)
[63] Mikelsons K and Freericks J K 2011 *Phys. Rev. A* **83** 043609
[64] Schnyder A P, Ryu S, Furusaki A and Ludwig A W W 2008 *Phys. Rev. B* **78** 195125
[65] Hasan M Z and Kane C L 2010 *Rev. Mod. Phys.* **82** 3045
[66] Qi X L and Zhang S C 2011 *Rev. Mod. Phys.* **83** 1057

[67] Chiu C K, Teo J C Y, Schnyder A P and Ryu S 2016 *Rev. Mod. Phys.* **88** 035005
[68] Aidelsburger M 2016 *Artificial Gauge Fields with Ultracold Atoms in Optical Lattices* (London: Springer)
[69] Bruun G M and Taylor E 2008 *Phys. Rev. Lett.* **101** 245301
[70] Duarte P M, Hart R A, Yang T L, Liu X, Paiva T, Khatami E, Scalettar R T, Trivedi N and Hulet R G 2015 *Phys. Rev. Lett.* **114** 070403
[71] Jiang S J and Zhou F 2015 *Phys. Rev. A* **92** 013619
[72] Emin D and Hart C F 1987 *Phys. Rev. B* **36** 2530
[73] Greiner M, Regal C A, Stewart J T and Jin D S 2005 *Phys. Rev. Lett.* **94** 110401
[74] Fölling S, Gerbier F, Widera A, Mandel O, Gericke T and Bloch I 2005 *Nature* **434** 481
[75] Rom T, Best T, Oosten D V, Schneider U, Fölling S, Paredes B and Bloch I 2006 *Nature* **444** 733
[76] Spielman I B, Phillips W D and Porto J V 2007 *Phys. Rev. Lett.* **98** 080404